

Non-Orthogonal Multiple Access for mmWave Drone Networks with Limited Feedback

Nadisanka Rupasinghe, Yavuz Yapıcı and İsmail Güvenç

Abstract

Unmanned aerial vehicle (UAV)-aided wireless communication networks can be a smart solution to provide connectivity during temporary events and after disasters. However, achieving high spectral efficiency is of paramount importance for UAVs due to limited energy resources on board of a UAV. In this paper, we introduce non-orthogonal multiple access (NOMA) transmission for UAVs serving as aerial base stations (BSs) at a large stadium potentially with several hundreds or thousands of mobile users. In particular, considering millimeter-wave (mmWave) transmission, we make use of multi-antenna techniques to generate directional beams specifically taking into consideration the physical constraints of the antenna array. Multiple users are served simultaneously within the same beam employing NOMA techniques. We focus on a limited feedback scheme in which user distances are considered for user ordering during NOMA formulation. For each user participating in NOMA, a target rate based on their quality of service (QoS) requirements is defined and UAV-BS hovering altitude is optimized to serve more users at their requested target rates. We develop a comprehensive framework over which outage probabilities and respective sum rates are derived rigorously for the distance feedback mechanism, which are verified through extensive simulations. Our analytical and simulation results depict that NOMA with distance feedback can provide better outage sum rates compared to its orthogonal counterpart. We investigate the optimal operation altitude of UAV-BS to maximize the sum rates using the tools of developed analytical framework. The importance of identifying a proper user pair for maximizing sum rates with NOMA transmission is also investigated.

Index Terms

drone, HPPP, mmWave, non-orthogonal multiple access (NOMA), stadium, UAV.

N. Rupasinghe, Y. Yapıcı, and İ. Güvenç are with the Department of Electrical and Computer Engineering, North Carolina State University, Raleigh, NC, 27606 (e-mail: {rprupasi, yyapici, iguvenç}@ncsu.edu).

I. INTRODUCTION

Unmanned aerial vehicle (UAV)-aided wireless communication networks are currently receiving high attention due to their possibility of rapid deployment during temporary events [1]–[4]. This rapid deployment is plausible mainly because they do not require fixed infrastructure for operation. Deploying a communication network without fixed infrastructure is extremely important when providing connectivity during natural disasters, terrorist attacks where existing communication infrastructure is destroyed [2], and serving temporary hot spot areas such as providing coverage to a stadium where thousands of mobile users are gathered [4].

When an UAV-aided communication network is deployed to provide broadband connectivity to mobile users in a stadium, achieving higher spectral efficiency (SE) is of utmost importance. In that case, integrating non-orthogonal multiple access (NOMA) which is identified as a promising technology for the next generation wireless communication systems [5], [6] due to its high SE, to UAV-aided communication network can be a smart solution. In contrast to the conventional orthogonal multiple access (OMA) schemes (e.g., time-division multiple access (TDMA)), NOMA simultaneously serves multiple users in non-orthogonal resources (in time, frequency, code and space domains) by separating the users in the power domain. Therefore, it is a suitable technology for effectively serving large number of wireless users, which is the case in large stadiums [4], [7] while enhancing SE.

In [5], a system-level performance evaluation based on 3GPP settings is carried out to identify potential performance gains with NOMA over orthogonal frequency division multiple access (OFDMA). Achievable performance with NOMA when users are randomly deployed is investigated in [8] considering two different criteria: 1) when each user has a targeted rate based on their quality-of-service (QoS) requirements; and 2) opportunistic user rates based on their channel conditions. Provided that the system parameters are appropriately chosen, better rate performance can be observed with NOMA compared to its orthogonal counterpart under both criteria. In [9], a power allocation strategy for NOMA transmission is discussed considering user fairness in the downlink (DL) data transmission. A cooperative NOMA strategy is proposed in [10] where strong users act as relays for weaker users with poor channel conditions to enhance their reception reliability. In [11], multiple-input-multiple-output (MIMO) techniques are introduced to NOMA transmission along with user pairing and power allocation strategies to enhance MIMO-NOMA performance over MIMO-OMA. A general MIMO-NOMA framework applicable to both DL

and uplink (UL) transmission is proposed in [12] by considering signal alignment concepts. In [7], a random beamforming approach for millimeter (mmWave) NOMA networks is proposed. To achieve power domain user separation, effective channel gains of users which depend on the angle offset between the randomly generated base station (BS) beam and user locations are considered. Two users are then served simultaneously within a single BS beam by employing NOMA techniques.

There are different techniques proposed in the literature to deploy UAVs serving as aerial BSs in a communication network, considering different criteria. In [13], multi-antenna techniques are exploited to develop an approach to optimize hovering locations of UAV-BS focusing on minimizing interference leakage and maximizing desired user signal-to-noise ratio (SNR). By optimizing UAV locations through brute force searching techniques [2] discusses achievable throughput coverage and 5th percentile SE gains from the deployment of UAV-BSs during disaster situations where existing fixed communication infrastructure is damaged. In a follow up work [14], further enhanced inter-cell interference coordination (FeICIC) from 3GPP Release 11 is introduced along with genetic algorithm based UAV hovering optimization technique to improve achievable 5th percentile SE further. In [15], by considering circle packing theory concepts, 3-Dimensional (3D) locations for deploying UAV-BSs with the objective of maximizing total coverage area is discussed. Impact of UAVs' altitude on the minimum required transmit power to achieve maximum ground coverage is analyzed in [16] for the case of two UAVs. An approach to identify hovering locations for UAVs in order to achieve power efficient DL transmission while satisfying the users' rate requirements is discussed in [17]. In [18], a method to identify 3D hovering locations for UAV-BSs is proposed with the objective of maximizing the revenue of the network which is measured considering the number of users covered by the UAV-BS. A UAV based mobile cloud computing system is proposed in [19] where UAVs offer computation offloading opportunities to mobile stations (MS) with limited local processing capabilities. In that, just for offloading purposes between UAV and MSs, NOMA is proposed as one viable solution. None of these earlier works consider deploying UAV-aided communication networks based on NOMA criteria.

In this paper, we consider a densely packed multi-user scenario where a UAV-BS is deployed to provide coverage over a large stadium or concert area. In order to improve spectral efficiency, we consider the NOMA strategy to serve multiple users simultaneously, and the respective mobile traffic can be offloaded efficiently. Our specific contributions are as follows.

- i. We first specify the coverage problem considering the relative size of the region where users are distributed and the physically radiated region, depending on the operational altitude of UAV-BS and the vertical beamwidth of the antenna propagation pattern. We show that the required vertical beamwidth to cover the entire user region is a concave function of the altitude, and, hence, the user region is partially covered for a range of altitudes of practical importance for UAV operations.
- ii. A beam scanning approach is proposed as an optimization problem to find the best location of the radiated region when the user region is covered only partially. We identify all unique events having various combinations of the presence of desired users within the physically radiated region, and formulate a hybrid transmission strategy serving all or part of desired users at a time based on the availability of desired users.
- iii. We consider NOMA transmission to increase spectral efficiency, and propose a practical feedback mechanism leveraging the user distance information, which has a potential to reduce overall complexity especially for rapidly fluctuating time-varying channels. We develop a comprehensive framework over which outage probabilities and respective sum rates are derived rigorously for this distance feedback mechanism, which are verified through extensive simulations. We also investigate the optimal operation altitude of UAV-BS to maximize the sum rates using the tools of developed analytical framework.

The rest of the paper is organized as follows. Section II captures the system model involving the NOMA transmission within a single UAV-BS DL beam. Formulation of NOMA transmission strategy is discussed in Section III, while outage probabilities and sum rates of NOMA with distance feedback are analytically investigated in Section IV. The respective numerical results are presented in Section V, and the paper ends with some concluding remarks in Section VI.

Notations: $(\cdot)^H$ denotes the Hermitian operation. δ_{ab} is the Kronecker delta function taking 1 if $a = b$, and 0 otherwise.

II. SYSTEM MODEL

We consider a mmWave-NOMA transmission scenario where a single UAV-BS, which is equipped with an M element antenna array, is serving mobile users in the DL. We assume that all these single-antenna users lie inside a specific *user region* as shown in Fig. 1, and are represented by the index set $\mathcal{N}_U = \{1, 2, \dots, K\}$. We also assume that the user region of interest may or may not be fully covered by a 3-dimensional (3D) beam generated by the UAV-BS

depending on the specific geometry of the environment and 3D antenna radiation pattern. In the specific scenario sketched in Fig. 1, only a smaller portion of the user region is being covered by the UAV-BS beam, and, hence, is labeled as *radiated region*. The user region is identified by inner-radius L_1 , outer-radius L_2 , and 2Δ , which is the fixed angle within the projection of horizontal beamwidth of the antenna pattern on the xy -plane, as shown in Fig. 1. Similarly, the radiated region is described by the inner-radius l_1 , outer-radius l_2 , and angle 2Δ . Note that it is possible to reasonably model various different hot spot scenarios such as a stadium, concert hall, traffic jam, and urban canyon by modifying these control parameters. For example, larger L_1 may correspond to a sports event where users are only allowed to use the available seats

in the tribunes while smaller L_1 may represent a music concert event where users can also be present on the ground as well as the tribunes.

A. User Distribution and mmWave Channel Model

We assume that mobile users are randomly distributed following a homogeneous Poisson point process (HPPP) with density λ [20], [21]. Hence, the number of users in the specified user region is Poisson distributed such that $P(K \text{ users in the user region}) = \frac{\mu^K e^{-\mu}}{K!}$ with $\mu = (L_2^2 - L_1^2)\Delta\lambda$. The channel \mathbf{h}_k between the k -th user in the user region and the UAV-BS is given as

$$\mathbf{h}_k = \sqrt{M} \sum_{p=1}^{N_P} \frac{\alpha_{k,p} \mathbf{a}(\theta_{k,p})}{\sqrt{\text{PL}(\sqrt{d_k^2 + h^2})}}, \quad (1)$$

where N_P , h , d_k , $\alpha_{k,p}$ and $\theta_{k,p}$ represent the number of multi-paths, UAV-BS hovering altitude, horizontal distance between k -th user and UAV-BS, gain of the p -th path which is complex Gaussian distributed with $\mathcal{CN}(0, 1)$, and angle-of-departure (AoD) of the p -th path, respectively, and $\mathbf{a}(\theta_{k,p})$ is the steering vector corresponding to AoD $\theta_{k,p}$ which is given for uniform linear array (ULA) as follows

$$\mathbf{a}(\theta_{k,p}) = \left[1 \quad e^{-j2\pi \frac{D}{\lambda} \sin(\theta_{k,p})} \quad \dots \quad e^{-j2\pi \frac{D}{\lambda} (M-1) \sin(\theta_{k,p})} \right]^T, \quad (2)$$

where D is the antenna spacing in the ULA, and λ is the wavelength. The path loss (PL) between k -th mobile user and UAV-BS is captured by $\text{PL}(\sqrt{d_k^2 + h^2})$. Without any loss of generality, we assume that all the users have line-of-sight (LoS) paths since UAV-BS is hovering at relatively high altitudes and the probability of having scatterers around UAV-BS is very small. Furthermore, as discussed in [7], [22], the effect of LoS link is dominant compared to Non-LoS (NLoS) links for mmWave frequency bands. Hence, it is reasonable to assume a single LoS path for the channel under consideration, and (1) accordingly becomes

$$\mathbf{h}_k = \sqrt{M} \frac{\alpha_k \mathbf{a}(\theta_k)}{\sqrt{\text{PL}(\sqrt{d_k^2 + h^2})}}, \quad (3)$$

where θ_k is AoD of the LoS path.

B. Coverage of User Region

Because of the limited vertical beamwidth φ_e of UAV-BS antenna radiation pattern, as in the sketch of Fig. 1, it may not be possible to cover the entire user region all the time. To gain

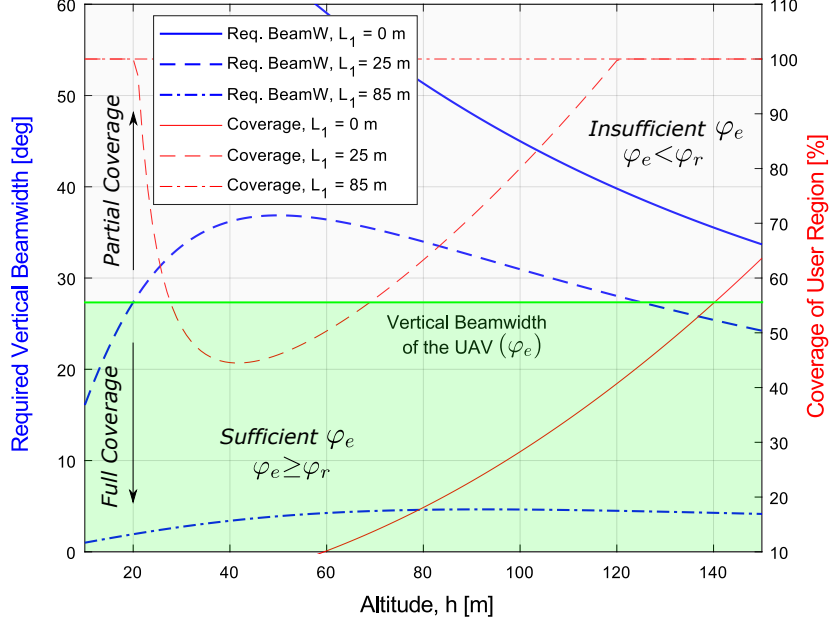


Fig. 2: Required vertical beamwidth φ_r to cover the entire user region, and percentage of the user region covered by the UAV with vertical beamwidth of $\varphi_e = 28^\circ$ are depicted along with varying UAV altitude and user deployment choices ($L_1 = \{0, 25, 85\}$ m, $L_2 = 100$ m). The upper and lower parts denote *insufficient* φ_e ($\varphi_e < \varphi_r$) and *sufficient* φ_e ($\varphi_e \geq \varphi_r$) regions, respectively, with respect to φ_r , where the user region is partially and fully covered, respectively.

more insight into this *partial coverage* problem, we depict the required vertical angle φ_r , which is demanded to cover the entire user region, in Fig. 2 along with varying UAV altitudes. In order to investigate the effect of various user deployment settings, as well, we consider three different inner radius L_1 values while keeping the outer radius L_2 the same (see Fig. 1 for relative geometry). We also show the percentage of the area radiated within the user region by the UAV-BS beam considering a vertical beamwidth of $\varphi_e = 28^\circ$. As can be seen from Fig. 2, two regions demarcated by vertical beamwidth φ_e , can be identified for the required beamwidth based on the achievable coverage within the user region. In particular, the region denoted as *insufficient* φ_e in the upper part of Fig. 2 corresponds to the case where $\varphi_e < \varphi_r$ and hence user region is covered only partially. On the other hand, the region denoted as *sufficient* φ_e in the lower part of Fig. 2 captures the case where user region is fully covered with $\varphi_e \geq \varphi_r$.

When the users are located everywhere in the stadium corresponding to the setting $L_1 = 0$ m,

the required vertical angle φ_r is very large and decreases monotonically with increasing UAV altitude, as depicted in Fig. 2. This intuitive result shows that the practical values of vertical beamwidth φ_e is incapable of covering the entire user region within the given UAV altitude range. However, when the inner-radius of the user region gets larger, which may be the case where there is a big stage in the middle of the stadium during a musical concert and is emulated by the setting $L_1 = 25$ m, the required vertical angle φ_r to cover the whole user region first increases at low UAV altitudes and then starts to decrease. Because of this non-monotonic convex type behavior, practical values of φ_e may not be sufficiently large to cover the entire user region at all possible altitudes.

As an example, the radiated region associated with $\varphi_e = 28^\circ$ and $L_1 = 25$ m is observed to cover the user region partially over the altitude range of $h \in [21, 120]$ m where we have $\varphi_e < \varphi_r$. Indeed, this altitude range is particularly important for the UAV-BS operation, since hovering at lower altitudes ($h < 20$ m) is not recommended due to safety issues while higher altitudes ($h > 120$ m) is restricted due to regulations of authorities in charge [23]. When the inner radius is made even larger, say $L_1 = 85$ m corresponding to a regular match setting of a stadium where users are allowed to seat only in tribunes, as can be seen from Fig. 2 the vertical beamwidth required to cover the entire user region is relatively small. These intuitive results show that achievable coverage over the user region heavily depends on the interaction among the vertical beamwidth of the UAV-BS beam, user deployment setting, and the operational altitude of UAV-BS, which will be investigated rigorously in the subsequent sections.

C. Beam Scanning over User Region

When the physically radiated region by the UAV-BS beam is smaller than the desired user region, it may matter which portion of the user region should be covered in the DL transmission. By changing the vertical tilting angle of the antenna array, the intersection point of the boresight direction of the UAV beam and the horizontal plane can be moved radially forward (towards outer radius) and backward (towards inner radius), as shown in Fig. 1. This way, it is possible to change the average path loss and radiated region size, both of which are affecting to the user sum rate. It is therefore of particular interest to search for an optimal intersection point or, equivalently, coverage within the user region for a given vertical beamwidth, φ_e which is insufficient to cover the entire user region ($\varphi_e < \varphi_r$).

We assume that the distance to the boresight intersection point from the origin is represented by D . Keeping the radiated region fully inside the user region, we define D_1 and D_2 to be the two extreme values of D where the inner-most and the outer-most portions of the user region are being covered, respectively, as in Fig. 1. As a result, D_1 corresponds to the radiated region where $l_1 = L_1$ and $l_2 < L_2$, whereas D_2 corresponds to the scenario of $l_1 > L_1$ and $l_2 = L_2$. With this, our proposed beam scanning strategy aims to find the optimum boresight intersection point D^* , or equivalently, the optimal coverage, such that the NOMA sum rates are maximized at a given altitude h . This can be formulated as follows

$$D^* = \underset{D_1 \leq D \leq D_2}{\operatorname{argmax}} R^{\text{NOMA}}, \quad (4)$$

where $D_1 = h \tan(\tan^{-1}(L_1/h) + \varphi_e/2)$ and $D_2 = h \tan(\tan^{-1}(L_1/h) - \varphi_e/2)$ via the geometry of Fig. 1, and R^{NOMA} is the NOMA sum rate. The optimum boresight intersection point D^* yields the optimum downward tilting angle as well for UAV-BS transmission at the given altitude.

III. NOMA FOR UAV-BS DOWNLINK

In this section, we consider NOMA transmission to serve multiple users simultaneously, which are called NOMA users hereafter, using a single DL beam of UAV-BS as sketched in Fig. 1. Assuming that each user has its own QoS based target rate, we evaluate respective sum rates to investigate conditions to serve each user at least at its target rate.

A. Outage Probabilities and Sum Rates for NOMA

In order to investigate sum rates for NOMA transmission, we first evaluate outage probability of each user individually, which captures the probability of a user being served at a rate less than its target rate. The sum rates are then computed as the weighted sum of target rates, where each target rate is weighted by its non-outage probability, and, hence, are called *outage* sum rates. To this end, we first characterize the effective channel gains for each user, which will then be used to derive instantaneous rates and outage probabilities.

We assume that the single UAV-BS may be assigned to either the entire environment where users are distributed, e.g., a stadium, or a part of it, e.g., a sector of a stadium. The AoD $\bar{\theta}$ of the beam \mathbf{b} generated by UAV-BS is therefore assumed to take values either from $[0, 2\pi]$, or a subset of it. In addition, the full coverage of the entire environment can be performed by choosing values for $\bar{\theta}$ from its support either sequentially or randomly over time. Without

any loss of generality, the effective channel gain of user $k \in \mathcal{N}_U$ for a particular beamforming direction $\bar{\theta}$ of UAV beam \mathbf{b} is given using (1) as follows

$$|\mathbf{h}_k^H \mathbf{b}|^2 = M \frac{|\alpha_k|^2 |\mathbf{b}^H \mathbf{a}(\theta_k)|^2}{\text{PL}(\sqrt{d_k^2 + h^2})} = \frac{|\alpha_k|^2}{\text{PL}(\sqrt{d_k^2 + h^2})} \left| \frac{\sin\left(\frac{\pi M(\sin \bar{\theta} - \sin \theta_k)}{2}\right)}{M \sin\left(\frac{\pi(\sin \bar{\theta} - \sin \theta_k)}{2}\right)} \right|^2 \quad (5)$$

where we assume a critically spaced ULA. Following the convention of [7], we assume small 2Δ while analyzing sum rates, i.e., $2\Delta \rightarrow 0$, which results in small angular offset such that $|\bar{\theta} - \theta_k| \rightarrow 0$. Choosing the coordinate system appropriately, small angular offset always implies small individual angles such that $\sin \bar{\theta} \rightarrow \bar{\theta}$ and $\sin \theta_k \rightarrow \theta_k$, and (5) can be approximated as

$$|\mathbf{h}_k^H \mathbf{b}|^2 \approx \frac{|\alpha_k|^2}{\text{PL}(\sqrt{d_k^2 + h^2})} \left| \frac{\sin\left(\frac{\pi M(\bar{\theta} - \theta_k)}{2}\right)}{M \sin\left(\frac{\pi(\bar{\theta} - \theta_k)}{2}\right)} \right|^2 = \frac{|\alpha_k|^2}{\text{PL}(\sqrt{d_k^2 + h^2})} F_M(\bar{\theta} - \theta_k), \quad (6)$$

where $F_M(\cdot)$ is called Fejér kernel. From (6) we can observe that the effective channel gain of user k depends on the offset of its angle θ_k from the beamforming direction $\bar{\theta}$, horizontal distance d_k to the UAV-BS, and the path gain α_k .

Note that NOMA transmission suggests to allocate power to each NOMA user in a way inversely proportional to its channel quality, and therefore requires the ordering of users based on their channel qualities. Deferring the discussion of user ordering strategies to the next section, we assume without any loss of generality that the users in set \mathcal{N}_U are already indexed from the worst to the best channel quality under a given criterion. Defining β_k to be the power allocation coefficient of k -th user, we therefore have $\beta_1 \geq \dots \geq \beta_K$ such that $\sum_{k=1}^K \beta_k^2 = 1$. The transmitted signal \mathbf{x} is then generated by superposition coding as follows

$$\mathbf{x} = \sqrt{P_{\text{Tx}}} \mathbf{b} \sum_{k=1}^K \beta_k s_k \quad (7)$$

where P_{Tx} and s_k are the total DL transmit power and k -th user's message, respectively. With (7), received signal at k th user is given as

$$y_k = \mathbf{h}_k^H \mathbf{x} + v_k = \sqrt{P_{\text{Tx}}} \mathbf{h}_k^H \mathbf{b} \sum_{k=1}^K \beta_k s_k + v_k, \quad (8)$$

where v_k is zero-mean complex Gaussian additive white noise with variance N_0 .

Adopting successive interference cancellation (SIC) approach, k -th user first decodes messages of weaker users (allocated with larger power) in the presence of stronger users' messages

(allocated with smaller power), and then subtracts decoded messages from its received signal y_k in (8). Thus, at k -th user, message intended to user m will be decoded with the following SINR

$$\text{SINR}_{m \rightarrow k} = \frac{P_{\text{Tx}} |\mathbf{h}_k^H \mathbf{b}|^2 \beta_m^2}{P_{\text{Tx}} \sum_{l=m+1}^K |\mathbf{h}_k^H \mathbf{b}|^2 \beta_l^2 + N_0}, \quad (9)$$

where $1 \leq m \leq k-1$. Assuming that all interfering messages of weaker users are decoded accurately, which requires the instantaneous rate associated with decoding any of these weaker users' messages to be larger than the respective target rate of that user, k -th user has the following SINR while decoding its own message

$$\text{SINR}_k = \frac{P_{\text{Tx}} |\mathbf{h}_k^H \mathbf{b}|^2 \beta_k^2}{(1 - \delta_{kK}) P_{\text{Tx}} \sum_{l=k+1}^K |\mathbf{h}_k^H \mathbf{b}|^2 \beta_l^2 + N_0}. \quad (10)$$

Next, we study how to evaluate outage probabilities and then outage sum rates using SINR terms in (9) and (10) considering different NOMA formulation criteria.

Defining the instantaneous rates associated with (9) and (10) to be $R_{m \rightarrow k} = \log_2(1 + \text{SINR}_{m \rightarrow k})$ and $R_k = \log_2(1 + \text{SINR}_k)$, respectively, the outage probability of k -th NOMA user is given as

$$\mathbf{P}_k^o = 1 - \mathbf{P}(R_{1 \rightarrow k} > \bar{R}_1, \dots, R_{k-1 \rightarrow k} > \bar{R}_{k-1}, R_k > \bar{R}_k | \mathcal{S}_K) \quad (11)$$

$$= 1 - \mathbf{P}(\text{SINR}_{1 \rightarrow k} > \epsilon_1, \dots, \text{SINR}_{k-1 \rightarrow k} > \epsilon_{k-1}, \text{SINR}_k > \epsilon_k | \mathcal{S}_K), \quad (12)$$

where \bar{R}_k is the QoS based target rate for k -th user and $\epsilon_k = 2^{\bar{R}_k} - 1$. Note that (11) and (12) are defined for \mathcal{S}_K describing the given condition on K which might involve either a range of integers, i.e., $\mathcal{S}_K: \{K | j \leq K < i\}$, or a unique integer, i.e., $\mathcal{S}_K: \{K | K = i\}$, where $i, j \in \mathbb{Z}^+$.

When \mathcal{S}_K denotes a unique K value, the outage sum rate is given as

$$R^{\text{NOMA}} = \mathbf{P}(K = 1) \left(1 - \tilde{\mathbf{P}}_1^o\right) \bar{R}_1 + \sum_{n=2}^{\infty} \mathbf{P}(K = n) \left(\sum_{k=1}^n (1 - \mathbf{P}_k^o) \bar{R}_k \right), \quad (13)$$

where $\tilde{\mathbf{P}}_k^o = \mathbf{P}\left(\frac{1}{K} \log(1 + P_{\text{Tx}} |\mathbf{h}_k^H \mathbf{b}|^2 / N_0) < \bar{R}_k | \mathcal{S}_K\right)$ is the outage probability of k -th user during OMA transmission with the factor $\frac{1}{K}$ capturing the loss of degrees-of-freedom (DoF) gain due to OMA. For performance comparison, we consider OMA sum rates which is computed same as (13) except substituting \mathbf{P}_k^o in the inner summation with $\tilde{\mathbf{P}}_k^o$.

Similarly, when we have the set $\mathcal{S}_K: \{K | j \leq K < i\}$, the outage sum rate is

$$R^{\text{NOMA}} = \sum_{k=1}^K (1 - \mathbf{P}_k^o) \bar{R}_k, \quad (14)$$

where $K \in \mathcal{S}_K$. Note that whenever we have $K = 1$, single user transmission is employed where the full time-frequency resources and transmit power are allocated to the scheduled user. Note also that OMA sum rates can be readily computed by using (14) and replacing P_k^o with \tilde{P}_k^o .

B. Full CSI and Distance Feedback

Since NOMA transmitter allocates power to NOMA users based on their channel qualities, it needs to order users according to their effective channel gains, which requires feedback of the full CSI of each user. Following the convention of the previous section, this order is given as

$$|\mathbf{h}_1^H \mathbf{b}|^2 \leq |\mathbf{h}_2^H \mathbf{b}|^2 \leq \dots \leq |\mathbf{h}_K^H \mathbf{b}|^2. \quad (15)$$

where the indices of users in set \mathcal{N}_U are arranged, without any loss of generality, such that user k has the k -th smallest effective channel gain. As a result, i -th user has a weaker channel quality than j -th user with $i < j$, which meets the power allocation strategy $\beta_i \geq \beta_j$ of Section III-A.

When the underlying channel experiences rapid fluctuations over time, tracking of CSI becomes computationally inefficient, and frequently sending this information back to the transmitter increases overhead. Note that the horizontal distance is one factor directly affecting the channel quality as shown in (6), and does not vary fast as compared to the effective channel gain. Thus, we consider to use distance information as a practical alternative of full CSI for ordering users. Since the effective channel gain is inversely proportional to horizontal distance as in (6), the following order is assumed for this *limited feedback* scheme

$$d_1 \leq d_2 \leq \dots \leq d_K. \quad (16)$$

With this order, i th user has still weaker channel quality than j th user, but this time with $i > j$, and we have still the same power allocation $\beta_i \geq \beta_j$. In addition, formulation of outage probabilities and sum rates of Section III-A applies to the distance feedback scheme, as well. However, the indices in set \mathcal{N}_U are now representing users ordered from the best to the worst channel quality such that user k is assumed to have the k th best channel quality.

C. Multiple Access For Partial Coverage

When the required vertical beamwidth is greater than the available UAV-BS vertical beamwidth, i.e., $\varphi_r > \varphi_e$, the user region is covered partially, and we explore the optimal position for the radiated region within the user region through beam scanning approach, as described in

Section II-C. Note that it might not be possible to find desired NOMA users in the radiated region when the user region is partially covered. In the following, we will elaborate all possible conditions for the presence of NOMA users within the radiated region considering i -th and j -th users only, though results can be generalized to multiple NOMA users as well.

Denoting the set of users inside the radiated region by \mathcal{N}_U^D , we identify four possible mutually exclusive events for the presence of the i -th and j -th users within the radiated region as follows

- *Event 1* (E_1): Both users are outside the radiated region ($i, j \notin \mathcal{N}_U^D$),
- *Event 2* (E_2): Only i -th user is within the radiated region ($i \in \mathcal{N}_U^D, j \notin \mathcal{N}_U^D$),
- *Event 3* (E_3): Only j -th user is within the radiated region ($j \in \mathcal{N}_U^D, i \notin \mathcal{N}_U^D$),
- *Event 4* (E_4): Both users are within the radiated region ($i, j \in \mathcal{N}_U^D$).

We modify the NOMA transmission strategy based on these four possible events as follows. The original NOMA is applicable only for E_4 since it is the only case having both users within the radiated region. When E_2 or E_3 occurs, i th or j th user, respectively, will be served all the time with full transmit power, which is therefore called single user transmission, and is common to OMA with the same outage probability. And, finally, no DL transmission will take place for E_1 as both users will be in outage. The overall transmission strategy is referred to as *hybrid NOMA*, which highlights the fact that UAV-BS employs NOMA whenever both users are available, and switches to single user transmission if a single NOMA user is present in the radiated region.

IV. NOMA OUTAGE SUM RATE WITH DISTANCE FEEDBACK

In this section, we will provide analytical expressions for the outage sum rate of NOMA transmission strategy described in Section III-C, when distance feedback is employed. We consider to serve i th and j users only with $i > j$, which are designated as the weaker and stronger users, respectively, and results can be generalized to multiple NOMA users, as well. We first formulate the outage sum rate expression based on events of Section III-C and respective outage probabilities, and then derive all these probability expressions assuming number of users to satisfy $j \leq K < i$ and $K \geq i$, in sequence.

A. Outage Sum Rate Formulation

We first formulate outage sum rate expression for NOMA transmission based on events of captured in Section III-C and respective outage probabilities, for i -th and j -th users with $i > j$. Hence, there should be at least j users in the user region to start transmission, and $K \geq j$. We

will evaluate the overall performance by individually considering the number of users K to be in the set $\mathcal{S}_{K_1} : \{K \mid j < K \leq i\}$ and $\mathcal{S}_{K_2} : \{K \mid K \geq i\}$ separately, and then combine them statistically to yield the desired result for $K \geq j$.

TABLE I: Possible NOMA Events with Nonzero Probability.

	$\mathcal{S}_{K_1} : j \leq K < i$	$\mathcal{S}_{K_2} : K \geq i$
$\varphi_e < \varphi_r$	E_1, E_3	E_1, E_2, E_3, E_4
$\varphi_e \geq \varphi_r$	E_3	E_4

In Table I, we list all possible NOMA events with nonzero probability based on the number of users, and the status of user region coverage. As an example, we have only j -th user for $j \leq K < i$, which might or might not be present in the radiated region captured by the events E_3 and E_1 , respectively, when the user region is partially covered with $\varphi_e < \varphi_r$. Note that, whenever the user region is fully covered with $\varphi_e \geq \varphi_r$, E_3 and E_4 are the only possible events for \mathcal{S}_{K_1} and \mathcal{S}_{K_2} , respectively, hence respective event probabilities are 1. We therefore consider the derivation of event probabilities only when the user region is partially covered.

The general expression for outage sum rates is therefore given as

$$R^{\text{NOMA}} = P\{\mathcal{S}_{K_1}\} \left[P\{E_3\} \left(1 - P_{j|\mathcal{S}_{K_1}}^{\text{o},3}\right) \bar{R}_j \right] + P\{\mathcal{S}_{K_2}\} \left[P\{E_2\} \left(1 - P_{i|\mathcal{S}_{K_2}}^{\text{o},2}\right) \bar{R}_i \right. \\ \left. + P\{E_3\} \left(1 - P_{j|\mathcal{S}_{K_2}}^{\text{o},3}\right) \bar{R}_j + P\{E_4\} \left(\left(1 - P_{i|\mathcal{S}_{K_2}}^{\text{o},4}\right) \bar{R}_i + \left(1 - P_{j|\mathcal{S}_{K_2}}^{\text{o},4}\right) \bar{R}_j \right) \right], \quad (17)$$

where $P\{\mathcal{S}_{K_1}\}$ and $P\{\mathcal{S}_{K_2}\}$ represent the probability of having K users in the user region given by \mathcal{S}_{K_1} and \mathcal{S}_{K_2} , respectively, $P\{E_n\}$ is the probability of event n , and $P_{k|\mathcal{S}_{K_l}}^{\text{o},n}$ is the *conditional* outage probability of k -th user for a given event n and set \mathcal{S}_{K_l} , with $k \in \{i, j\}$, $n \in \{2, 3, 4\}$, and $l \in \{1, 2\}$. Note that, (17) is applicable to both full and partial coverage of user region through suitable event probabilities such that $P\{E_2\} = P\{E_3\} = 0$ and $P\{E_3\} = P\{E_4\} = 1$ under full coverage. Since we consider a range of K values, (17) can be rearranged to yield (14), where the overall *unconditional* outage probabilities of i -th and j -th users are given as

$$P_j^{\text{o}} = 1 - \left[P\{\mathcal{S}_{K_1}\} P\{E_3\} \left(1 - P_{j|\mathcal{S}_{K_1}}^{\text{o},3}\right) \right. \\ \left. + P\{\mathcal{S}_{K_2}\} \left\{ P\{E_3\} \left(1 - P_{j|\mathcal{S}_{K_2}}^{\text{o},3}\right) + P\{E_4\} \left(1 - P_{j|\mathcal{S}_{K_2}}^{\text{o},4}\right) \right\} \right], \quad (18)$$

$$P_i^{\text{o}} = 1 - P\{\mathcal{S}_{K_2}\} \left[P\{E_2\} \left(1 - P_{i|\mathcal{S}_{K_2}}^{\text{o},2}\right) + P\{E_4\} \left(1 - P_{i|\mathcal{S}_{K_2}}^{\text{o},4}\right) \right], \quad (19)$$

and, outage sum rates of (14) and (17) can be calculated as $R^{\text{NOMA}} = P_i^o \bar{R}_i + P_j^o \bar{R}_j$. In the subsequent sections, we derive analytical expressions for event probabilities $P\{E_n\}$ under partial coverage of user region, and conditional outage probabilities $P_{k|\mathcal{S}_{K_l}}^{o,n}$ given in (17) for the sets \mathcal{S}_{K_1} and \mathcal{S}_{K_2} , in sequence, assuming both coverage status.

B. Event and Conditional Outage Probabilities for \mathcal{S}_{K_1}

In order to analytically evaluate event and conditional outage probabilities in (17) for \mathcal{S}_{K_1} , we first consider the marginal PDF of the k -th user distance conditioned on \mathcal{S}_{K_1} .

Theorem 1: Assuming that the number of users K is chosen from the set \mathcal{S}_{K_1} such that $j \leq K < i$, the marginal PDF of the k th user distance d_k is given as

$$f_{d_k|\mathcal{S}_{K_1}}(r_k) = \frac{2\Delta\lambda r_k}{\mathcal{C}} e^{-\Delta(L_2^2 - L_1^2)\lambda} \frac{[\Delta(r_k^2 - L_1^2)\lambda]^{(k-1)}}{(k-1)!} \left(\sum_{l=0}^{i-k-1} \frac{[\Delta(L_2^2 - r_k^2)\lambda]^l}{l!} \right) \quad (20)$$

where $\mathcal{C} = \sum_{l=j}^{i-1} \frac{e^{-\Delta(L_2^2 - L_1^2)\lambda} [\Delta(L_2^2 - L_1^2)\lambda]^l}{l!}$.

Proof: See Appendix A. ■

Since this particular case assumes the presence of only j -th user and no i -th user at all, the possible events are E_1 and E_3 , as shown in Table I. As there is no transmission for E_1 , we focus on E_3 in this particular case. For partially covered user region with $\varphi_e < \varphi_r$, E_3 happens when j -th user lies in the radiated region, and d_j is lying in $l_1 \leq d_j \leq l_2$ (see Fig. 1). Employing (20), desired event probability is calculated as

$$P\{E_3\} = P\{l_1 \leq d_j \leq l_2 | \mathcal{S}_{K_1}\} = \int_{l_1}^{l_2} f_{d_j|\mathcal{S}_{K_1}}(r) dr. \quad (21)$$

Employing (10) and (12), conditional outage probability for this particular case is given as

$$P_{j|\mathcal{S}_{K_1}}^{o,3} = P\left\{|\mathbf{h}_j^H \mathbf{b}|^2 < \eta_j \mid E_3\right\} = \frac{1}{P\{E_3\}} P\left\{|\mathbf{h}_j^H \mathbf{b}|^2 < \eta_j, l_{\min} \leq d_j \leq l_{\max} \mid \mathcal{S}_{K_1}\right\}, \quad (22)$$

$$= \frac{1}{P\{E_3\}} \int_{\mathcal{D}_\theta} P\left\{|\mathbf{h}_j^H \mathbf{b}|^2 < \eta_j, l_{\min} \leq d_j \leq l_{\max} \mid x_j, \mathcal{S}_{K_1}\right\} f_{x_j}(x) dx, \quad (23)$$

where $f_{x_j}(x)$ is the PDF of j -th user location x_j , \mathcal{D}_θ denotes the radiated region, and $\eta_j = \frac{\epsilon_j}{P_{\text{Tx}}/N_0}$. Note that both full and partial coverage of the user region is considered in (22) by choosing d_j

interval with the limits $l_{\min} = \max(L_1, l_1)$ and $l_{\max} = \min(l_2, L_2)$. Since x_j is fully specified by distance d_j and angle θ_j , which are independent of each other, (23) can be represented as

$$P_{j|\mathcal{S}_{K_1}}^{o,3} = \frac{1}{P\{E_3\}} \int_{\bar{\theta}-\Delta}^{\bar{\theta}+\Delta} \int_{l_1}^{l_2} P\left\{|\mathbf{h}_j^H \mathbf{b}|^2 < \eta_j \mid d_j = r, \theta_j = \theta\right\} \frac{f_{d_j|\mathcal{S}_{K_1}}(r)}{2\Delta} dr d\theta, \quad (24)$$

$$= \frac{1}{P\{E_3\}} \int_{\bar{\theta}-\Delta}^{\bar{\theta}+\Delta} \int_{l_1}^{l_2} \left(1 - \exp\left\{-\frac{\eta_j \text{PL}(\sqrt{r^2 + h^2})}{F_M(\bar{\theta} - \theta_j)}\right\}\right) \frac{f_{d_j|\mathcal{S}_{K_1}}(r)}{2\Delta} dr d\theta, \quad (25)$$

where we assume a uniform distribution for θ_j within $[\bar{\theta} - \Delta, \bar{\theta} + \Delta]$, and employ distribution of $|\mathbf{h}_j^H \mathbf{b}|^2$ which is exponential for a given location since path gain α_k is complex Gaussian.

C. Event and Conditional Outage Probabilities for \mathcal{S}_{K_2}

We now consider event and conditional outage probabilities for \mathcal{S}_{K_2} , where we assume the presence of both i -th and j -th users. We therefore need the joint PDF of user distances d_i and d_j , which is given in the following theorem.

Theorem 2: Assuming that the number of users K is chosen from the set \mathcal{S}_{K_2} such that $K \geq i$, the joint PDF of i th and j th user distances d_i and d_j , respectively, with $d_j \leq d_i$, is given as

$$f_{d_j, d_i|\mathcal{S}_{K_2}}(r_k, r_i) = \frac{(2\Delta\lambda)^2}{\mathcal{C}} r_k r_i e^{-\Delta(r_k^2 - L_1^2)\lambda} \frac{[\Delta(r_k^2 - L_1^2)\lambda]^{(j-1)}}{(j-1)!} \frac{[\Delta(r_i^2 - r_k^2)\lambda]^{(i-j-1)}}{(i-j-1)!} \quad (26)$$

where $\mathcal{C} = 1 - \sum_{l=0}^{i-1} \frac{e^{-\Delta(L_2^2 - L_1^2)\lambda} [\Delta(L_2^2 - L_1^2)\lambda]^l}{l!}$.

Proof: See Appendix B. ■

For this particular case, we derive probabilities of E_2 , E_3 , and E_4 when the user region is partially covered with $\varphi_e < \varphi_r$, as shown in Table I. We first consider E_2 where we have only i -th user in the radiated region such that $l_1 \leq d_i \leq l_2$ (see Fig. 1), and j -th user should be outside the radiated region. Given $d_j \leq d_i$, which comes from user ordering of Section III-B, the only possible d_j interval is $L_1 \leq d_j \leq l_1$. The respective event probability is therefore given as

$$P\{E_2\} = P\{L_1 \leq d_j \leq l_1, l_1 \leq d_i \leq l_2, d_j \leq d_i \mid \mathcal{S}_{K_2}\} = \int_{l_1}^{l_2} \int_{L_1}^{l_1} f_{d_j, d_i|\mathcal{S}_{K_2}}(r, \ell) dr d\ell. \quad (27)$$

Similarly, any event E_n can be represented as $\{a_n \leq d_j \leq b_n, u_n \leq d_i \leq v_n \mid \mathcal{S}_{K_2}\}$, such that

$$P\{E_n\} = \int_{u_n}^{v_n} \int_{a_n}^{b_n} f_{d_j, d_i|\mathcal{S}_{K_2}}(r, \ell) dr d\ell, \quad (28)$$

where $n \in \{2, 3, 4\}$, and the integral limits are given as

$$(a_n, b_n, u_n, v_n) = \begin{cases} (L_1, l_1, l_1, l_2) & \text{if } n = 2 \\ (l_1, l_2, l_2, L_2) & \text{if } n = 3, \\ (l_{\min}, d_i, l_{\min}, l_{\max}) & \text{if } n = 4 \end{cases} \quad (29)$$

where $l_{\min} = \max(L_1, l_1)$ and $l_{\max} = \min(l_2, L_2)$ make sure the validity of (29) for full coverage of the user region, which will be employed during outage computation in the sequel.

Following the strategy of (22), conditional outage probabilities $P_{i|S_{K_2}}^{\circ,2}$, $P_{i|S_{K_2}}^{\circ,4}$, $P_{j|S_{K_2}}^{\circ,3}$, and $P_{j|S_{K_2}}^{\circ,4}$ of (17) can therefore be expressed as

$$\begin{aligned} P_{k|S_{K_2}}^{\circ,n} &= P \left\{ |\mathbf{h}_k^H \mathbf{b}|^2 < \eta_k^{(n)} \mid E_n \right\} = \frac{1}{P\{E_n\}} P \left\{ |\mathbf{h}_k^H \mathbf{b}|^2 < \eta_k^{(n)}, a_n \leq d_j \leq b_n, e_n \leq d_i \leq f_n \mid S_{K_2} \right\} \\ &= \frac{1}{P\{E_n\}} \int_{\mathcal{D}_\theta} P \left\{ |\mathbf{h}_k^H \mathbf{b}|^2 < \eta_k^{(n)}, a_n \leq d_j \leq b_n, e_n \leq d_i \leq f_n \mid x_k, S_{K_2} \right\} f_{x_k|S_{K_2}}(x) dx, \end{aligned}$$

where $\eta_k^{(n)}$ is given for $k \in \{i, j\}$, $n \in \{2, 3, 4\}$ as $\eta_i^{(2)} = \frac{\epsilon_i}{P_{\text{Tx}}/N_0}$, $\eta_j^{(3)} = \frac{\epsilon_j}{P_{\text{Tx}}/N_0}$, $\eta_i^{(4)} = \frac{\epsilon_i/(P_{\text{Tx}}/N_0)}{\beta_i^2 - \beta_j^2 \epsilon_i}$ and $\eta_j^{(4)} = \max \left\{ \frac{\epsilon_i/(P_{\text{Tx}}/N_0)}{\beta_i^2 - \beta_j^2 \epsilon_i}, \frac{\epsilon_j}{(P_{\text{Tx}}/N_0)\beta_j^2} \right\}$ [7]. Considering all possible d_i and d_j values, the desired conditional outage probabilities can be computed as follows

$$\begin{aligned} P_{k|S_{K_2}}^{\circ,n} &= \frac{1}{P\{E_n\}} \int_{\bar{\theta}-\Delta}^{\bar{\theta}+\Delta} \int_{e_n}^{f_n} \int_{a_n}^{b_n} P \left\{ |\mathbf{h}_k^H \mathbf{b}|^2 < \eta_k^{(n)} \mid d_j = r, d_i = \ell, \theta_k = \theta \right\} \frac{f_{d_j, d_i|S_{K_2}}(r, \ell)}{2\Delta} dr d\ell d\theta, \\ &= \frac{1}{P\{E_n\}} \int_{\bar{\theta}-\Delta}^{\bar{\theta}+\Delta} \int_{e_n}^{f_n} \int_{a_n}^{b_n} \left(1 - \exp \left\{ -\frac{\eta_k^{(n)} \text{PL}(\sqrt{\delta_{ki}\ell^2 + \delta_{kj}r^2 + h^2})}{F_M(\bar{\theta} - \theta_k)} \right\} \right) \frac{f_{d_j, d_i|S_{K_2}}(r, \ell)}{2\Delta} dr d\ell d\theta. \end{aligned} \quad (30)$$

V. NUMERICAL RESULTS

In this section, we study in detail achievable outage sum rates for NOMA and OMA transmissions. By making use of the derived analytical expressions in Section IV and through extensive computer simulations, we investigate optimal altitudes for UAV operation to maximize sum rates for the scenario discussed in Section II. We consider two path-loss models in our analysis: 1) distance dependent PL model given as $\text{PL}(\sqrt{d^2 + h^2}) = 1 + (\sqrt{d^2 + h^2})^\gamma$ [7], where γ is the path-loss exponent and d is the horizontal distance to UAV-BS, and 2) *close-in* (CI) free-space reference distance model for urban micro (UMi) mmWave environment given as $\text{PL}((\sqrt{d^2 + h^2}), f_c) = 32.4 + 21 \log_{10}(\sqrt{d^2 + h^2}) + 20 \log_{10}(f_c)$ [24], where f_c represents the operating mmWave frequency. The simulation parameters are summarized in Table II.

TABLE II: Simulation Parameters

Parameter	Value
User distribution	Uniform
Outer radius, L_2	100 m
Inner radius, L_1	25 m
Horizontal angular width, 2Δ	0.5°
Vertical beamwidth, φ_e	28°
HPPP density, λ	1
Number of BS antennas, M	10
Noise, N_0	-35 dBm
Path-loss exponent, γ	2
j th user target rate, \bar{R}_j	6 BPCU
i th user target rate, \bar{R}_i	0.5 BPCU
j th user power allocation, β_j^2	0.25
i th user power allocation, β_i^2	0.75
UAV-BS operation altitude, h	10 m - 150 m
mmWave operating frequency, f_c	30 GHz

A. Effect of Feedback Type: Distance vs. Full CSI Feedback

In Fig. 3 and Fig. 4, we depict sum rates and outage performances, respectively, for NOMA with full CSI and distance based feedback schemes. Considering the ordering schemes in Section III-B, full CSI feedback picks $i = K - 24$ and $j = K - 19$ while distance feedback assumes $i = 25$ and $j = 20$, in order to make sure users with the same order of channel quality are selected under two feedback schemes. We observe in Fig. 3 that sum rates improve along with the increasing transmit power for both feedback schemes, and that the better of these two feedback mechanisms depends on the operation altitude of UAV-BS and the transmit power. In particular, for smaller transmit power, $P_{Tx} = 10$ dBm, distance feedback scheme provides better sum rates compared to full CSI up to an altitude of 80 m. However, there is no performance difference for higher altitudes ($h > 80$ m). Note that, for this transmit power, j -th user is in complete outage, while i -th user has similar outage performance for both feedback schemes at high altitudes, as captured in Fig. 4. At a moderate transmit power of 20 dBm, full CSI feedback is superior to distance feedback up to 75 m, and falls short of it after that altitude level. Interestingly, for relatively higher transmit power of $P_{Tx} = 30$ dBm, we have an opposite behavior such that full CSI feedback is first inferior to distance feedback for altitudes up to 82.5 m, and beats it for higher altitudes. Although it will be discussed in more detail later on, we briefly note here that

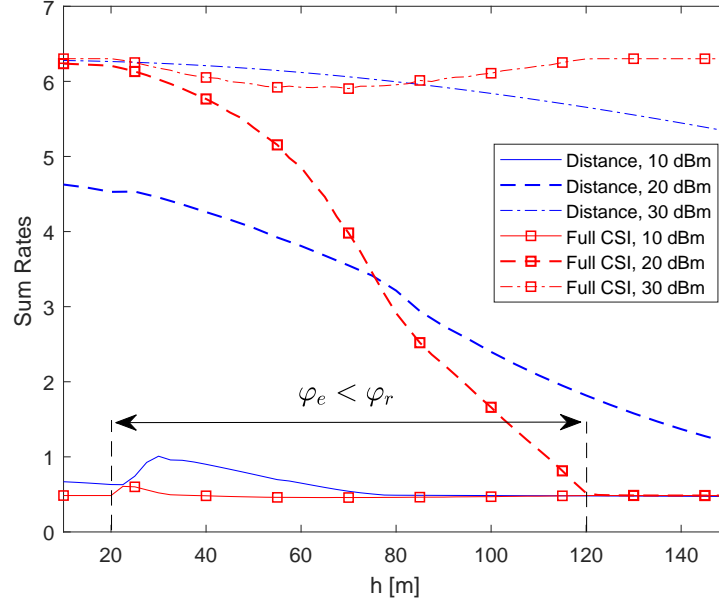
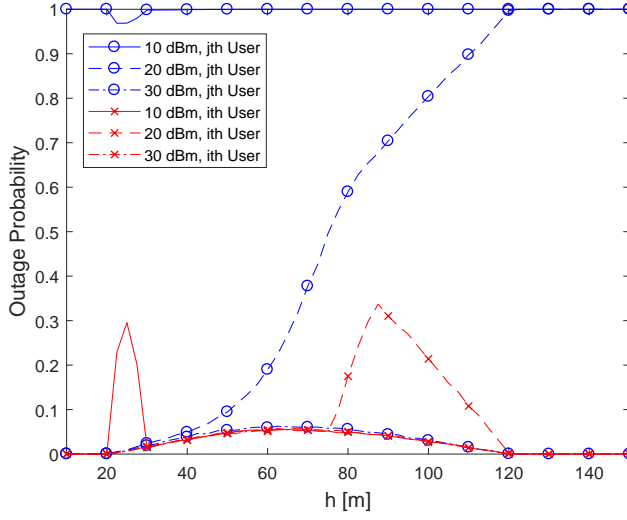


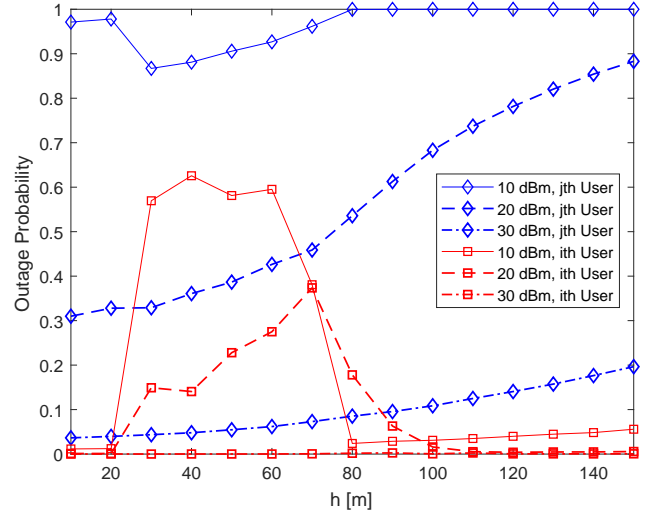
Fig. 3: Sum rates of NOMA with full CSI and distance feedback where $i = 25$, $j = 20$. Altitude range for partially covered user region is explicitly shown for which $\varphi_e < \varphi_r$.

the optimal altitude of UAV-BS is non-monotonically varying along with operation altitude for certain settings. For example, NOMA with distance feedback and $P_{Tx} = 10$ dBm achieves the best sum rate of 1 BPCU at $h = 30$ m.

An important point to note here is that, although distance feedback scheme lacks the information of actual channel quality which full CSI feedback exploits completely, its sum rate performance can sometimes be better, as seen in Fig. 3, and also mentioned in [7], [25]. The reason for this interesting result is the fact that distance feedback is not actually employing users with the fixed order of channel quality with respect to full CSI, or, equivalently, effective channel gain. Note that whenever distance order is not the same as full CSI order, distance feedback picks up users each time with a different *actual order*, which is the desired order with respect to effective channel gain. Since order of NOMA users directly affects outage and sum rates, distance feedback therefore achieves varying performance over trials, which may either be better or worse than that of full CSI depending on the transmission settings and distribution of actual order. To provide a better insight, we depict the simulation based PDF of actual indices (with respect to the actual order) of NOMA users in Fig. 5, whose indices are $i = 25$ and $j = 20$, based



(a) Full CSI Feedback



(b) Distance Feedback

Fig. 4: Outage of NOMA with full CSI and distance feedback, where $i = 25$ and $j = 20$ are for distance feedback while $i = K - 24$ and $j = K - 19$ with $K = 46$ are for full CSI feedback.

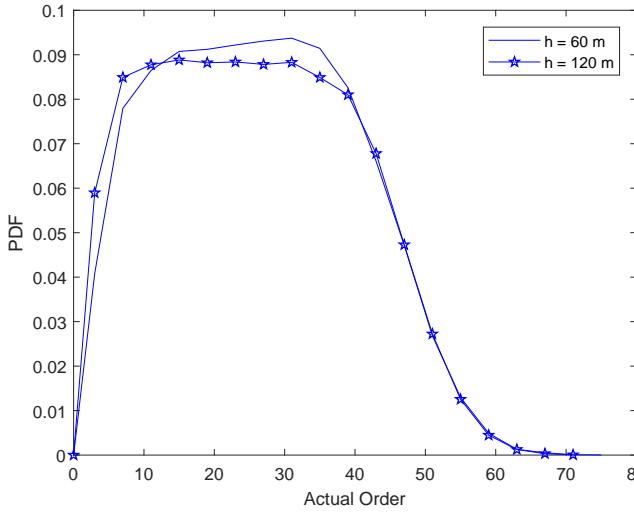
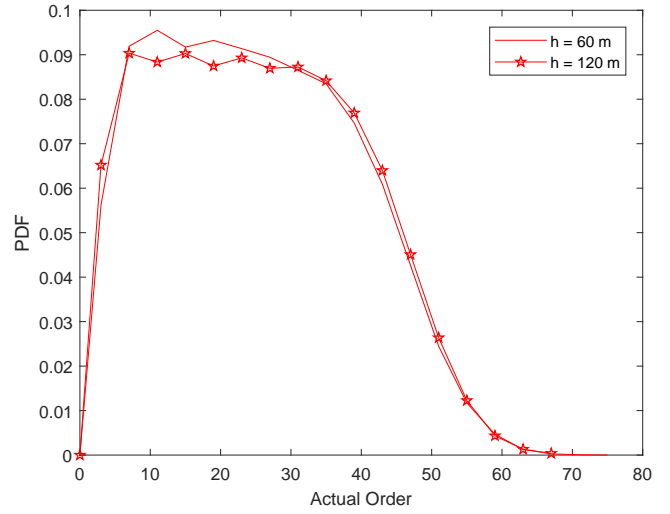
(a) i -th user(b) j -th user

Fig. 5: Distribution of actual order for distance feedback with $i = 25$, $j = 20$, and $h = \{60, 120\}$ m.

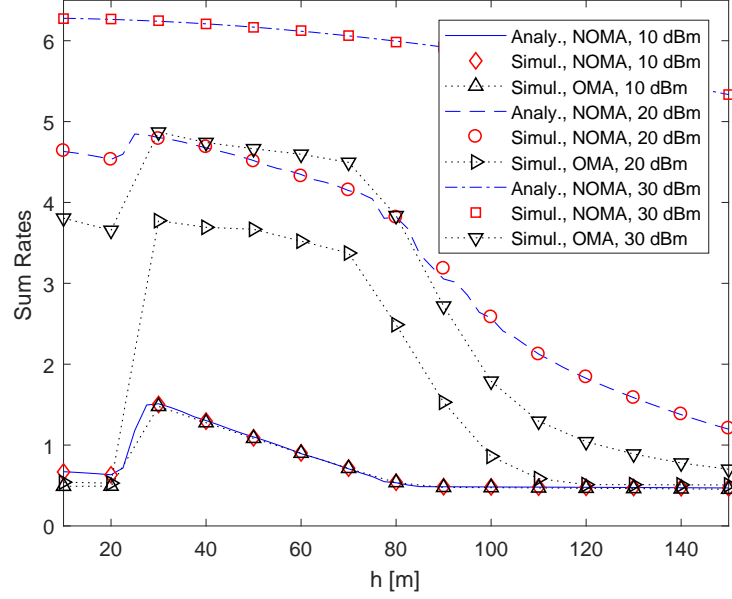


Fig. 6: Sum rates of OMA and NOMA with distance feedback where $i = 30$, $j = 20$.

on the distance based ordering. We observe that although i and j is fixed for distance based ordering, corresponding actual indices can take much different values.

B. Performance of Distance Feedback: NOMA vs. OMA

In Fig. 6, we present sum rate performance of OMA and NOMA for distance feedback scheme along with varying altitude, where $i = 30$ and $j = 20$. As can be observed, analytical sum rate results for NOMA perfectly match with the simulation based results. We observe that OMA and NOMA sum rate performance are very similar for $P_{Tx} = 10$ dBm, which is also observed from respective outage results of i -th and j -th users in Fig. 7. On the other hand, when the transmit power becomes 20 dBm or 30 dBm, sum rates of NOMA becomes significantly better than that of OMA, which is accompanied by relatively lower outage probabilities of both NOMA users as captured in Fig. 7.

We observe that sum rates are not monotonic with increasing altitude for the transmit power of 10 dBm and 20 dBm, and, hence, the optimal operation altitude of UAV-BS appears to be 27.5 m and 25 m, respectively, for those two transmit power values. Note that when the user region is fully covered ($h \leq 20$ m), both i -th and j -th users are present within the radiated region

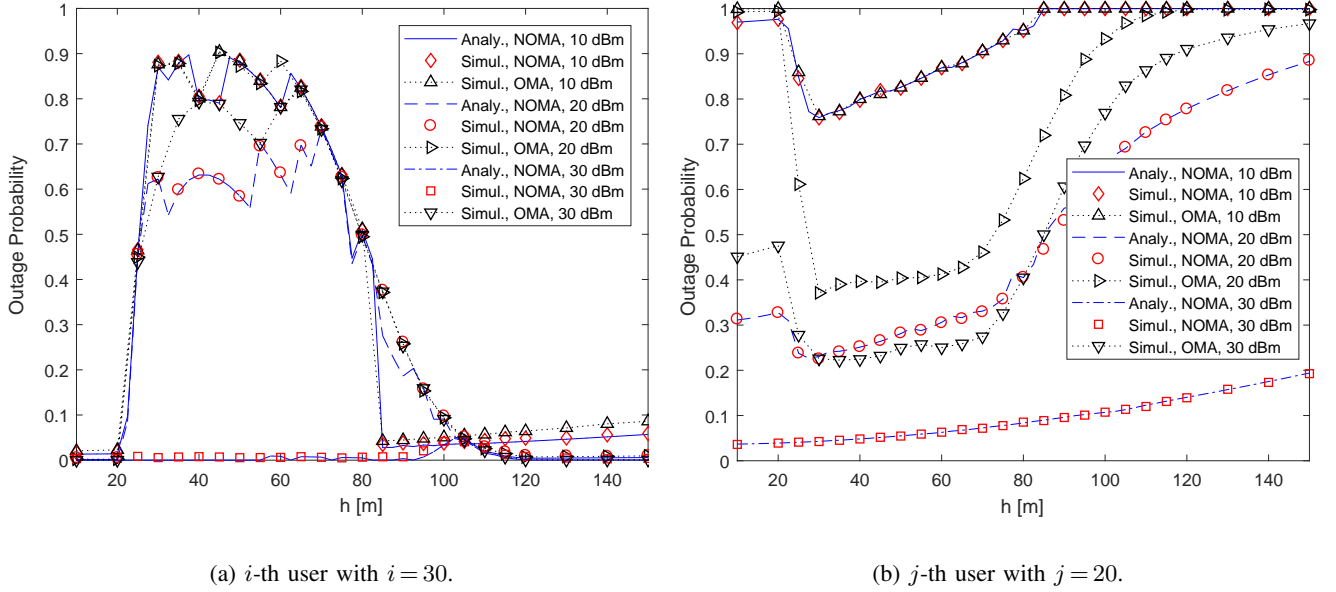


Fig. 7: Outage probability of OMA and NOMA with distance feedback.

($P\{E_4\} = 1$) and NOMA scheme tries to serve both of them. During this situation and with $P_{Tx} = 10$ dBm, the allocated power to j -th user is insufficient, and, hence, low target rate of i -th user dominates in the sum rates, i.e., at $h = 10$ m, $R^{NOMA} = 0.66$ BPCU. On the other hand, when $h \geq 20$ m, $P\{E_4\}$ starts decreasing rapidly due to the partial coverage of the user region whereas $P\{E_3\}$ starts increasing while enhancing the existence probability of only the j -th user within the radiated region, as captured in Fig. 8. Whenever j -th user is scheduled as the only user, single user transmission is realized as described in Section III-C, and hence the respective outage probability of j -th user decreases. The resulting sum rate is then dominated by the target rate of j -th user. Due to this reason, we observe a maximum sum rate value at a specific altitude and after that sum rates start decreasing due to the increasing PL and decreasing probability of finding j -th user, as shown in Fig. 8.

C. Effect of Beam Scanning and User Separation

In Fig. 9, we present the impact of beam scanning on the sum rate performance of NOMA with distance feedback along with the respective event probabilities considering $h = 50$ m, $i = 30$ and $j = 20$. As discussed in Section II-C, when $\varphi_r > \varphi_e$, through beam scanning the optimal value of boresight intersection point D is searched to identify the radiated region within the user

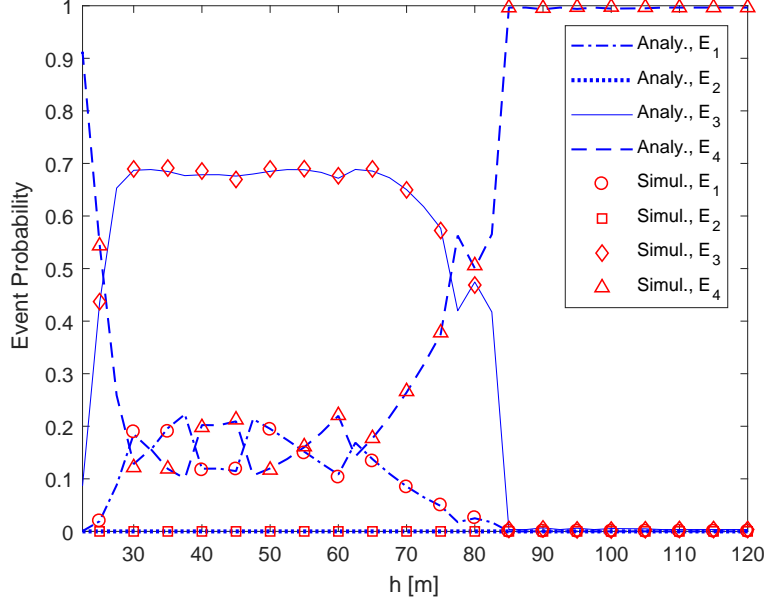


Fig. 8: Event probability variation for distance feedback scheme over the altitude range corresponding to partially covered user region. At each altitude, radiated region is identified via beam scanning as discussed in Section II-C. Here, $i = 30$, $j = 20$ and $P_{Tx} = 10$ dBm.

region. The possible D values vary between $D_1 = 42.8$ m and $D_2 = 58.4$ m to keep the radiated region within the user region boundaries. We observe that the optimal D is 45 m and 48 m for the transmit power of 10 dBm and 20 dBm, respectively, while any value $D \geq 53$ m seems suitable for the optimal operation with 30 dBm. Note that, conventional NOMA is more likely as D gets larger since finding both users is more probable, as can be observed from Fig. 9(b), event probability E_4 . In contrast, it is more likely to find only j -th user, represented by E_3 , for relatively smaller D values. As a result, whenever the transmit power is sufficient to serve j -th user at least at its target rate, large D values are preferred to benefit from NOMA. On the other hand, smaller D values corresponding to smaller $P\{E_4\}$ are better for low transmit power values to leverage transmission only to j -th user with full power.

We consider the effect of user separation after ordering them based on distances, on NOMA sum rates in Fig. 10, assuming $i = \{21, 25, 30\}$, $j = 20$, and transmit power of 20 dBm. We observe that increasing the user separation $|i - j|$ results in larger sum rates over the the altitude range corresponding to partially covered user region. This is because, when the user separation

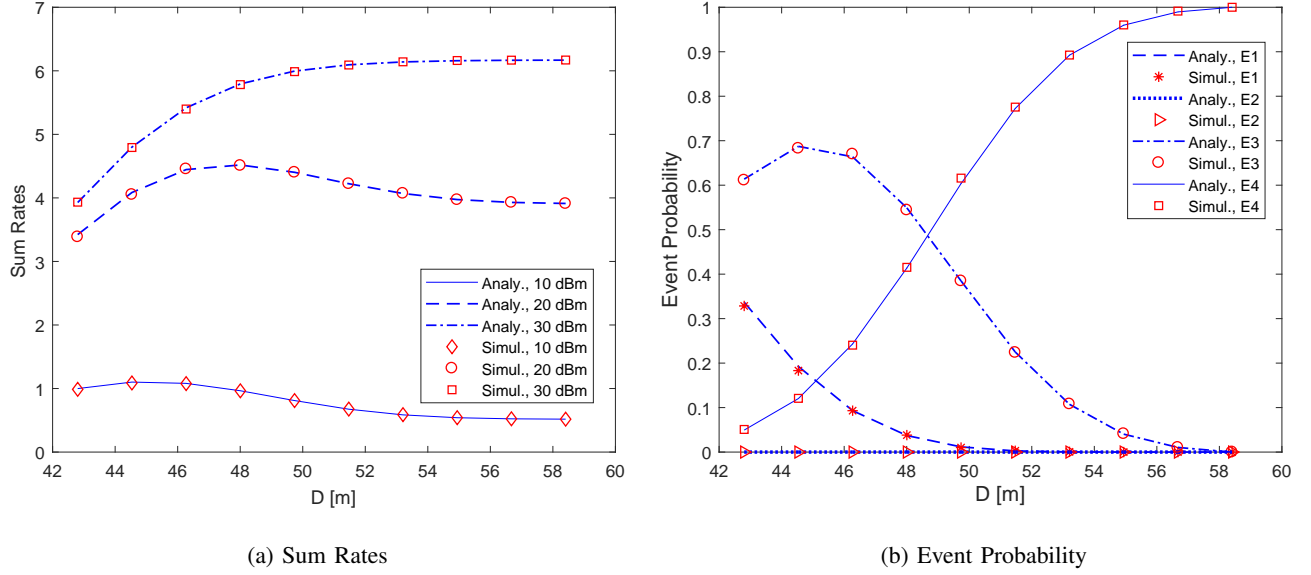


Fig. 9: Effect of beam scanning on NOMA sum rates together with event probabilities for $i = 30$, $j = 20$, and $h = 50$ m, where we assume distance feedback scheme.

is small, $P\{E_4\}$ increases since both users have similar distances and finding both of them within the radiated region is highly probable which result in serving both of them simultaneously using NOMA transmission. As discussed in Section V-C, with limited transmit power values, single user transmission is preferable over NOMA to achieve better outage sum rates. Hence, better outage sum rates are observed for larger i, j separation here mainly because of the single user transmission due to smaller $P\{E_4\}$.

We observe a maximum in sum rates around the altitude of 25 m for $i = 30$, from Fig. 10. As discussed previously and can be seen from Fig. 8 for $P\{E_3\}$, this is because, there is a higher chance of scheduling only the j -th user up to the altitude of 80 m. Due to the increasing PL, sum rates start to drop with a slower rate till 80 m. After 80 m sum rates drop with a higher rate due to the increasing of $P\{E_4\}$ as captured in Fig. 8.

D. NOMA Performance with mmWave PL Model

We finally investigate achievable sum rates and outage performance for OMA and NOMA with distance feedback scheme considering the CI mmWave path-loss model defined previously, and depict the respective results in Fig. 11 and Fig. 12, for $i = 25$ and $j = 20$. From Fig. 11 we

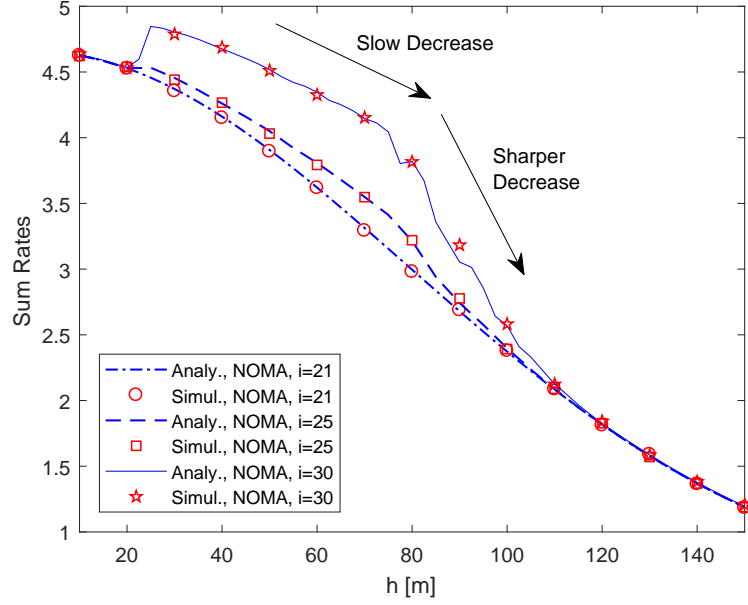


Fig. 10: Effect of user separation on NOMA sum rates with distance feedback for $i = \{21, 25, 30\}$, $j = 20$, and $P_{Tx} = 20$ dBm transmit power.

observe that analytical sum rate results for NOMA perfectly match with the simulation based results, as before, and that NOMA results are better than OMA except at $P_{Tx} = 60$ dBm. Due to the severe PL in mmWave frequency bands, the required transmit power level is observed to be relatively larger. It is worth remarking that, we consider $M = 100$, since it is reasonable to expect more antenna elements in the array for mmWave frequencies. This will provide a larger beamforming gain to partially compensate the severe PL. Similar to distance dependent path-loss model, with CI PL model also sum rates exhibit a maximum at the altitude of around 27.5 m for $P_{Tx} = 70$ dBm which is accompanied by the decrease in j -th user outage probabilities.

VI. CONCLUDING REMARKS

In this paper, we introduce NOMA transmission to a UAV-aided communication network which is deployed to provide coverage over a densely packed user region such as a stadium or a concert area. We show that the user region may not be covered at practical UAV-BS operation altitudes, which basically depends on the size of the entire user region, vertical beamwidth of the antenna propagation pattern, and the specific transmission geometry. We introduce a beam scanning

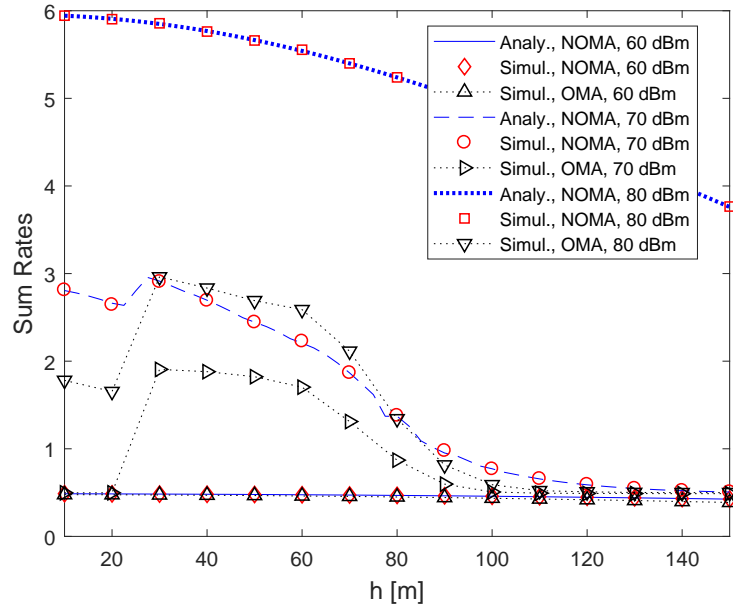
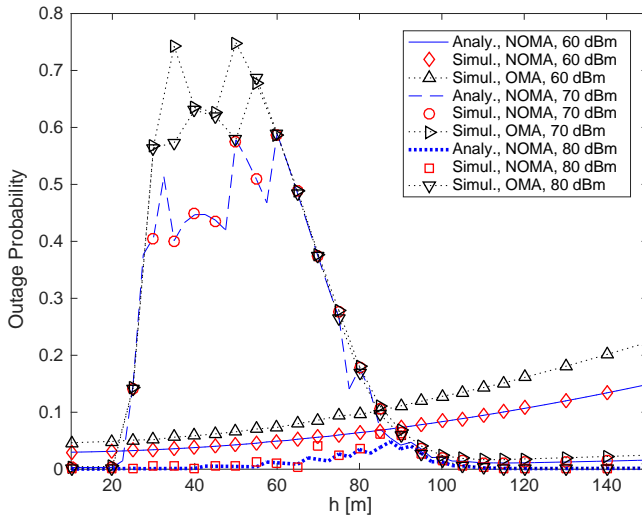
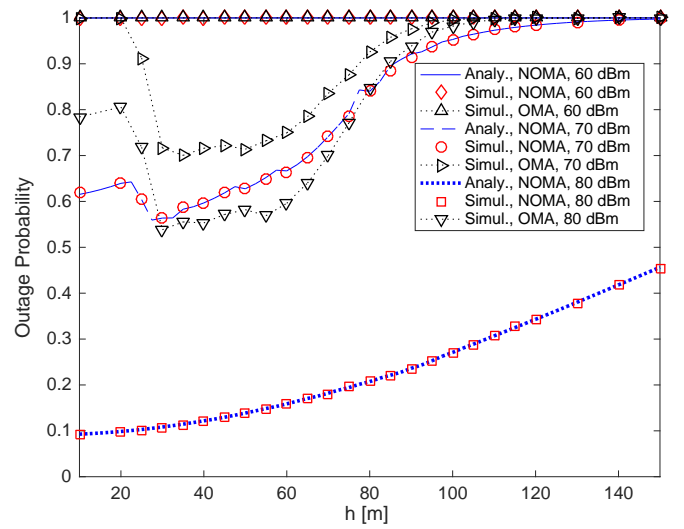


Fig. 11: Sum rates of OMA and NOMA with distance feedback for CI mmWave channel where $i = 25$, $j = 20$.



(a) i th user with $i = 25$



(b) j th user with $j = 20$

Fig. 12: Outage probability of OMA and NOMA with distance feedback for CI mmWave channel.

approach involving an optimization problem to identify the optimal area to be radiated within the user region when entire user region can not be covered completely. We accordingly propose a hybrid transmission strategy serving all or some of the desired users at a time, which leverages the presence of desired NOMA users in the radiated region. As a practical feedback mechanism, we consider the distance information while ordering users for NOMA formulation, which appears to be an efficient alternative for full CSI feedback especially for rapidly fluctuating channels. We develop a comprehensive framework to rigorously derive analytical expressions of respective outage probabilities and sum rates for the NOMA transmission under consideration with the distance feedback mechanism. The optimal operation altitude of UAV-BS is also investigated to maximize the achievable sum rates using the developed analytical framework.

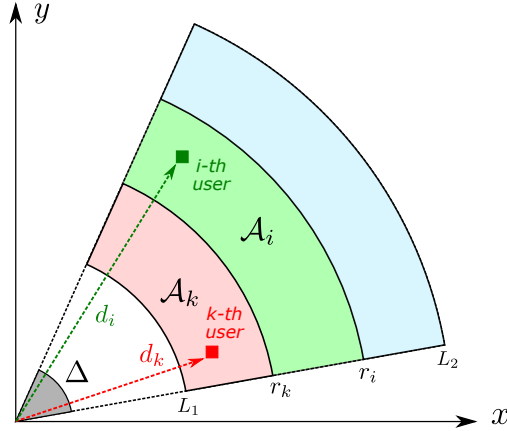


Fig. 13: Sketch of user region $\mathcal{A} = \Delta(L_2^2 - L_1^2)$ with $\mathcal{A}_k = \Delta(r_k^2 - L_1^2)$ and $\mathcal{A}_i = \Delta(r_i^2 - r_k^2)$.

APPENDIX A

THE MARGINAL PDF OF USER DISTANCES FOR \mathcal{S}_{K_1}

Let us first consider the cumulative distribution function (CDF) of the k -th user distance d_k assuming that K is chosen from $\mathcal{S}_{K_1} : \{K | j \leq K < i\}$, which is given as

$$F_{d_k|\mathcal{S}_{K_1}}(r_k) = \mathbb{P}\{d_k < r_k | j \leq K < i\} = \frac{\mathbb{P}\{d_k < r_k, j \leq K < i\}}{\mathbb{P}\{j \leq K < i\}}. \quad (31)$$

Note that while the denominator of (31) is readily available from the definition of HPPP, we will relate the ordered user distances to the number of users with a help of Fig. 13, as discussed in [20], in order to calculate the probability in the nominator. To this end, the first condition

$d_k < r_k$ in the numerator of (31) is interpreted as the necessity of the area \mathcal{A}_k having at least k users. In addition, given that the number of users in \mathcal{A}_k is $l \geq k$, the second condition $j \leq K < i$ requires that the remaining area $\mathcal{A} - \mathcal{A}_k$ has at most $(i - l - 1)$ users, so that the user region has less than i users. As a result, the desired probability is calculated as

$$\begin{aligned} \mathbb{P}\{d_k < r_k, j \leq K < i\} &= \sum_{l=k}^{i-1} \mathbb{P}\{\mathcal{A}_k \text{ has } l \text{ users, } \mathcal{A} - \mathcal{A}_k \text{ has at most } (i - l - 1) \text{ users}\} \\ &= \sum_{l=k}^{i-1} \frac{e^{-\Delta(r_k^2 - L_1^2)\lambda} [\Delta(r_k^2 - L_1^2)\lambda]^l}{l!} \left\{ \sum_{l'=0}^{i-l-1} \frac{e^{-\Delta(L_2^2 - r_k^2)\lambda} [\Delta(L_2^2 - r_k^2)\lambda]^{l'}}{l'!} \right\}. \end{aligned} \quad (32)$$

Using (32) and $\mathcal{C} = \mathbb{P}\{j \leq K < i\} = \sum_{l=j}^{i-1} \frac{e^{-\Delta(L_2^2 - L_1^2)\lambda} [\Delta(L_2^2 - L_1^2)\lambda]^l}{l!}$, the marginal CDF in (31) can be readily obtained. Finally, the marginal PDF can be obtained by taking derivative as follows

$$\begin{aligned} f_{d_k|\mathcal{S}_{K_1}}(r_k) &= \frac{\partial}{\partial r_k} F_{d_k|\mathcal{S}_{K_1}}(r_k) \\ &= \frac{e^{-\Delta(L_2^2 - L_1^2)\lambda}}{\mathcal{C}} \frac{\partial}{\partial r_k} \left\{ \sum_{l=k}^{i-1} \sum_{l'=0}^{i-l-1} \frac{[\Delta(r_k^2 - L_1^2)\lambda]^l}{l!} \frac{[\Delta(L_2^2 - r_k^2)\lambda]^{l'}}{l'!} \right\} \\ &= \frac{(2\Delta\lambda r_k) e^{-\Delta(L_2^2 - L_1^2)\lambda} [\Delta(r_k^2 - L_1^2)\lambda]^{(k-1)}}{\mathcal{C} (k-1)!} \left(\sum_{l=0}^{i-k-1} \frac{[\Delta(L_2^2 - r_k^2)\lambda]^l}{l!} \right). \quad \blacksquare \end{aligned} \quad (33)$$

APPENDIX B

THE JOINT PDF OF USER DISTANCES FOR \mathcal{S}_{K_2}

Similar to the marginal PDF derivation in Appendix A, we first consider the joint CDF of the user distances d_k and d_i with $d_k \leq d_i$ assuming that $K \in \mathcal{S}_{K_2}$ with $\mathcal{S}_{K_2} = \{K | K \geq i\}$, which is given as

$$F_{d_k, d_i|\mathcal{S}_{K_2}}(r_k, r_i) = \mathbb{P}\{d_k < r_k, d_i < r_i, d_k \leq d_i | K \geq i\} = \frac{\mathbb{P}\{d_k < r_k, d_i < r_i, d_k \leq d_i, K \geq i\}}{\mathbb{P}\{K \geq i\}}. \quad (34)$$

Considering the probability expression in the numerator of (34) and Fig. 13, \mathcal{A}_k should have at least k users to satisfy $d_k < r_k$. In addition, the condition $d_i < r_i$ requires the presence of at least i users in $\mathcal{A}_k + \mathcal{A}_i$, which also meets the condition $K \geq i$. Given that the number of users

in \mathcal{A}_k is $l \geq k$, \mathcal{A}_i has at least $(i - l)$ users. Note that, the maximum number of users in \mathcal{A}_k should be $(i-1)$ to satisfy $d_k \leq d_i$. The desired probability is accordingly given as

$$\begin{aligned} P\{d_k < r_k, d_i < r_i, d_k \leq d_i, K \leq i\} &= \sum_{l=k}^{i-1} P\{\mathcal{A}_k \text{ has at least } l \text{ users, } \mathcal{A}_i \text{ has at least } (i-l) \text{ users}\} \\ &= \sum_{l=k}^{i-1} \frac{e^{-\Delta(r^2 - L_1^2)\lambda} [\Delta(r^2 - L_1^2)\lambda]^l}{l!} \left\{ 1 - \sum_{l'=0}^{i-l-1} \frac{e^{-\Delta(r_i^2 - r^2)\lambda} [\Delta(r_i^2 - r^2)\lambda]^{l'}}{l'!} \right\}. \end{aligned} \quad (35)$$

Employing (35) and $\mathcal{C} = P\{K \geq i\} = 1 - \sum_{l=0}^{i-1} \frac{e^{-\Delta(L_2^2 - L_1^2)\lambda} [\Delta(L_2^2 - L_1^2)\lambda]^l}{l!}$, the joint CDF in (34) is readily available. Taking derivative of the joint CDF, we obtain the joint PDF as follows

$$\begin{aligned} f_{d_k, d_i | \mathcal{S}_{K_2}}(r, r_i) &= \frac{\partial^2 F_{d_k, d_i | \mathcal{S}_{K_2}}(r, r_i)}{\partial r \partial r_i} \\ &= -\frac{1}{\mathcal{C}} \frac{\partial}{\partial r_i} \left\{ \frac{\partial}{\partial r} \left\{ \sum_{l=k}^{i-1} \sum_{l'=0}^{i-l-1} \frac{e^{-\Delta(r_i^2 - L_1^2)\lambda} [\Delta(r^2 - L_1^2)\lambda]^l [\Delta(r_i^2 - r^2)\lambda]^{l'}}{l! l'!} \right\} \right\} \\ &= -\frac{1}{\mathcal{C}} \frac{\partial}{\partial r_i} \left\{ \frac{(2\Delta\lambda r) [\Delta(r^2 - L_1^2)\lambda]^{(k-1)}}{(k-1)!} e^{-\Delta(r_i^2 - L_1^2)\lambda} \sum_{l'=0}^{i-k-1} \frac{[\Delta(r_i^2 - r^2)\lambda]^{l'}}{l'!} \right\} \\ &= \frac{(2\Delta\lambda r)}{\mathcal{C}} \frac{[\Delta(r^2 - L_1^2)\lambda]^{(k-1)}}{(k-1)!} (2\Delta\lambda r_i) e^{-\Delta(r_i^2 - L_1^2)\lambda} \frac{[\Delta(r_i^2 - r^2)\lambda]^{(i-k-1)}}{(i-k-1)!}. \quad \blacksquare \end{aligned} \quad (36)$$

REFERENCES

- [1] Y. Zeng, R. Zhang, and T. J. Lim, "Wireless communications with unmanned aerial vehicles: opportunities and challenges," *IEEE Commun. Mag.*, vol. 54, no. 5, pp. 36–42, May 2016.
- [2] A. Merwaday, A. Tuncer, A. Kumbhar, and I. Guvenc, "Improved throughput coverage in natural disasters: Unmanned aerial base stations for public-safety communications," *IEEE Vehicular Technology Magazine*, vol. 11, no. 4, pp. 53–60, 2016.
- [3] V. Sharma, M. Bennis, and R. Kumar, "UAV-assisted heterogeneous networks for capacity enhancement," *IEEE Commun. Lett.*, vol. 20, no. 6, pp. 1207–1210, June 2016.
- [4] N. Rupasinghe, Y. Yapici, I. Guvenc, and Y. Kakishima, "Non-orthogonal multiple access for mmWave drones with multi-antenna transmission," in *Proc. Asilomar Conf. Sig., Sys. Comp.*, 2017.
- [5] Y. Saito, Y. Kishiyama, A. Benjebbour, T. Nakamura, A. Li, and K. Higuchi, "Non-orthogonal multiple access (NOMA) for cellular future radio access," in *Proc. IEEE Veh. Technol. Conf. (VTC)*, June 2013, pp. 1–5.
- [6] Technical Specification Group Radio Access Network, "Study on downlink multiuser superposition transmission (MUST) for LTE," 3rd Generation Partnership Project (3GPP), Tech. Rep. 3GPP TR36.859 v13.0.0, Dec. 2015.
- [7] Z. Ding, P. Fan, and H. V. Poor, "Random beamforming in millimeter-wave NOMA networks," *IEEE Access*, no. 99, pp. 1–1, 2017.
- [8] Z. Ding, Z. Yang, P. Fan, and H. V. Poor, "On the performance of non-orthogonal multiple access in 5G systems with randomly deployed users," *IEEE Sig. Process. Lett.*, vol. 21, no. 12, pp. 1501–1505, Dec. 2014.
- [9] S. Timotheou and I. Krikidis, "Fairness for non-orthogonal multiple access in 5G systems," *IEEE Sig. Process. Lett.*, vol. 22, no. 10, pp. 1647–1651, Oct. 2015.

- [10] Z. Ding, M. Peng, and H. V. Poor, "Cooperative non-orthogonal multiple access in 5G systems," *IEEE Commun. Lett.*, vol. 19, no. 8, pp. 1462–1465, Aug. 2015.
- [11] Z. Ding, F. Adachi, and H. V. Poor, "The application of MIMO to non-orthogonal multiple access," *IEEE Trans. Wireless Commun.*, vol. 15, no. 1, pp. 537–552, Jan. 2016.
- [12] Z. Ding, R. Schober, and H. V. Poor, "A general MIMO framework for NOMA downlink and uplink transmission based on signal alignment," *IEEE Trans. Wireless Commun.*, vol. 15, no. 6, June 2016.
- [13] N. Rupasinghe, A. S. Ibrahim, and I. Guvenc, "Optimum hovering locations with angular domain user separation for cooperative UAV networks," in *Proc. IEEE Global Commun. Conf. (GLOBECOM)*, Dec. 2016, pp. 1–6.
- [14] A. Kumbhar, I. Guvenc, S. Singh, and A. Tuncer, "Exploiting LTE-Advanced HetNets and FeICIC for UAV-assisted public safety communications," *IEEE Access*, vol. PP, no. 99, pp. 1–1, 2017.
- [15] M. Mozaffari, W. Saad, M. Bennis, and M. Debbah, "Efficient deployment of multiple unmanned aerial vehicles for optimal wireless coverage," *IEEE Commun. Lett.*, vol. 20, no. 8, pp. 1647–1650, Aug 2016.
- [16] —, "Drone small cells in the clouds: Design, deployment and performance analysis," in *Proc. IEEE Global Commun. Conf. (GLOBECOM)*, San Diego, CA, USA, Dec 2015, pp. 1–6.
- [17] —, "Optimal transport theory for power-efficient deployment of unmanned aerial vehicles," in *Proc. IEEE Int. Conf. on Commun. (ICC)*, May 2016, pp. 1–6.
- [18] R. I. Bor-Yaliniz, A. El-Keyi, and H. Yanikomeroglu, "Efficient 3-D placement of an aerial base station in next generation cellular networks," in *Proc IEEE Int.l Conf. on Commun. (ICC)*, May 2016, pp. 1–5.
- [19] S. Jeong, O. Simeone, and J. Kang, "Mobile edge computing via a uav-mounted cloudlet: Optimization of bit allocation and path planning," *IEEE Trans. Vehic. Technol.*, vol. PP, no. 99, pp. 1–1, 2017.
- [20] M. Haenggi, *Stochastic Geometry for Wireless Networks*. Cambridge Univ. Press, Cambridge, UK, 2012.
- [21] A. Merwaday, S. Mukherjee, and I. Güvenç, "Capacity analysis of LTE-Advanced HetNets with reduced power subframes and range expansion," *EURASIP Journal on Wireless Communications and Networking*, vol. 2014, no. 1, p. 189, 2014.
- [22] G. Lee, Y. Sung, and J. Seo, "Randomly-directional beamforming in millimeter-wave multiuser MISO downlink," *IEEE Trans. Wireless Commun.*, vol. 15, no. 2, pp. 1086–1100, Feb. 2016.
- [23] Federal Aviation Administration, "Summary of small unmanned aircraft rule," Jun. 2016. [Online]. Available: https://www.faa.gov/uas/media/Part_107_Summary.pdf
- [24] Aalto Uni., BUPT, CMCC, Ericsson, Huawei, Intel, KT Corporation, Nokia, NTT DOCOMO, New York Uni., Qualcomm, Samsung, Uni. of Bristol, and USC, "5G channel model for bands up to 100 GHz," White paper v2.2, Mar. 2016.
- [25] Y. Yapıcı and I. Güvenç, "NOMA for visible light communications with random receiver orientation," under review in *IEEE Int. Commun. Conf. (ICC)*, Jan. 2018.